LA-UR-15-20834
Approved for public release; distribution is unlimited.

Title: Observation of cyclotron resonance and electron-phonon coupling in surface states of the bulk-insulating topological insulator Cu0:02Bi2Se3

Author(s): Wu, Liang
Tse, Wang-Kong
Morris, C. M.
Brahlek, M.
Koirala, N.
Oh, S.
Armitage, N. P.

Intended for: Journal Physical Review Letters and Arxiv

Issued: 2015-02-05

# Supplemetary Information for "Cyclotron resonance and electron-phonon coupling on surface states of the bulk-insulating topological insulator $Cu_{0.02}Bi_2Se_3$"

Liang Wu,[1] Wang-Kong Tse,[2] C. M. Morris,[1] M. Brahlek,[3] N. Koirala,[3] S. Oh,[3] and N.P. Armitage[1,*]

[1]*The Institute for Quantum Matter, Department of Physics and Astronomy, The Johns Hopkins University, Baltimore, MD 21218 USA.*
[2]*Los Alamos National Laboratory, Los Alamos, NM 87545, USA*
[3]*Department of Physics and Astronomy, Rutgers the State University of New Jersey. Piscataway, NJ 08854*

## I. MATERIALS AND METHODS

Standard time-domain THz spectroscopy (TDTS) in a transmission geometry was performed with a custom home-built THz spectrometer. In this technique an approximately single-cycle picosecond pulse of light is transmitted through the sample and the substrate. The complex transmission is obtained from Fourier transforming the time-domain sample pulse and ratioing it to a Fourier transformed substrate pulse. The complex conductance can be directly inverted from the transmission equation in the thin film limit[1, 2]:

$$\tilde{T}(\omega) = \frac{1+n}{1+n+Z_0 G(\omega)} e^{i\omega/c(n-1)\Delta L} \tag{1}$$

where $\Delta L$ is the small difference in thickness between the sample and reference substrates, $n$ is the substrate index of refraction and $Z_0$ is the vacuum impedance, 376.7Ω. By measuring both the magnitude and phase of the transmission, this inversion to conductance is done directly and does not require Kramers-Kronig transformation.TDTS is an ideal tool to study the low frequency response of these materials with both the metallic Drude peak and a $E_{1u}$ infrared active phonon visible.

Thin films of $Bi_2Se_3$ were grown at Rutgers University by molecular beam epitaxy (MBE) on 0.5 mm thick crystalline $Al_2O_3$ substrates. Details on growth can be found elsewhere[3–5]. Films grow a quintuple layer (1 unit cell) at a time (1QL~1nm). After film growth, 100nm Se capping is deposited to prevent aging effects[6]. Se capping was shown to have a negligible contribution to the optics at THz frequencies [2], yet it serves a very important protection layer as Cu doped $Bi_2Se_3$ is much less stable in air than pure $Bi_2Se_3$. 3-4% optimal Cu concentration (Cu/Bi×100%) was incorporated during the film deposition and the concentration can be controlled at the better than 1% level. Therefore, the 'x' in $Cu_xBi_2Se_3$ formula is 0.015-0.02. Samples were sealed in vacuum and sent immediately to JHU and low temperature TDTS measurements began within 24 hours of their growth. The samples were mounted inside an optical helium flow cryostat and cooled down to 5K within an hour.

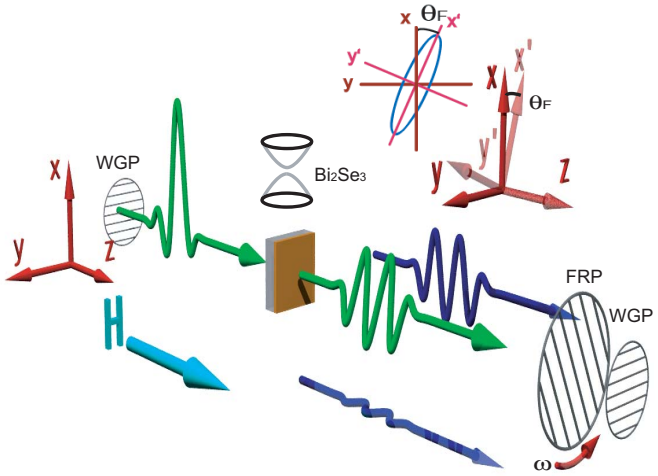


FIG. 1: (Color online) Demonstration of experimental setup for Faraday rotation experiments.

Complex Faraday rotation measurements were performed in a closed-cycle 7T superconducting magnet at 5K. We use the fast rotator technique to measure the polarization states accurately[7]. As shown in Fig.1 in the main text, a static wire-grid polarizer (WGP1) is placed before the sample. After the sample, a fast rotating polarizer (FRP) unit and another static WGP2 are used. WGP1 and WGP2 transmit vertically polarized light. With this combination, in the fast rotator technique, $E_{xx}(t)$ and $E_{xy}(t)$ (blue pulses)can be measured simultaneously in a single scan by reading off the in- and out-of-phase outputs from a lockin. Complex Faraday rotation $\theta_F = \theta_F^{'} + i\theta_F^{''}$can be obtained by $\theta_F$=atan($E_{xy}(\omega)/E_{xx}(\omega)$) after Fourier transforming into the frequency domain. Linearly polarized light becomes elliptically polarized after passing through the sample with a Faraday rotation $\theta_F^{'}$ (real part). The imaginary part of the Faraday rotation $\theta_F^{''}$ is close to ellipticityin the small rotation angle regime[7] . A small background rotation from misalignment was subtracted by measuring a blank substrate.

## II. MORE CYCLOTRON RESONANCE DATA AND FITS

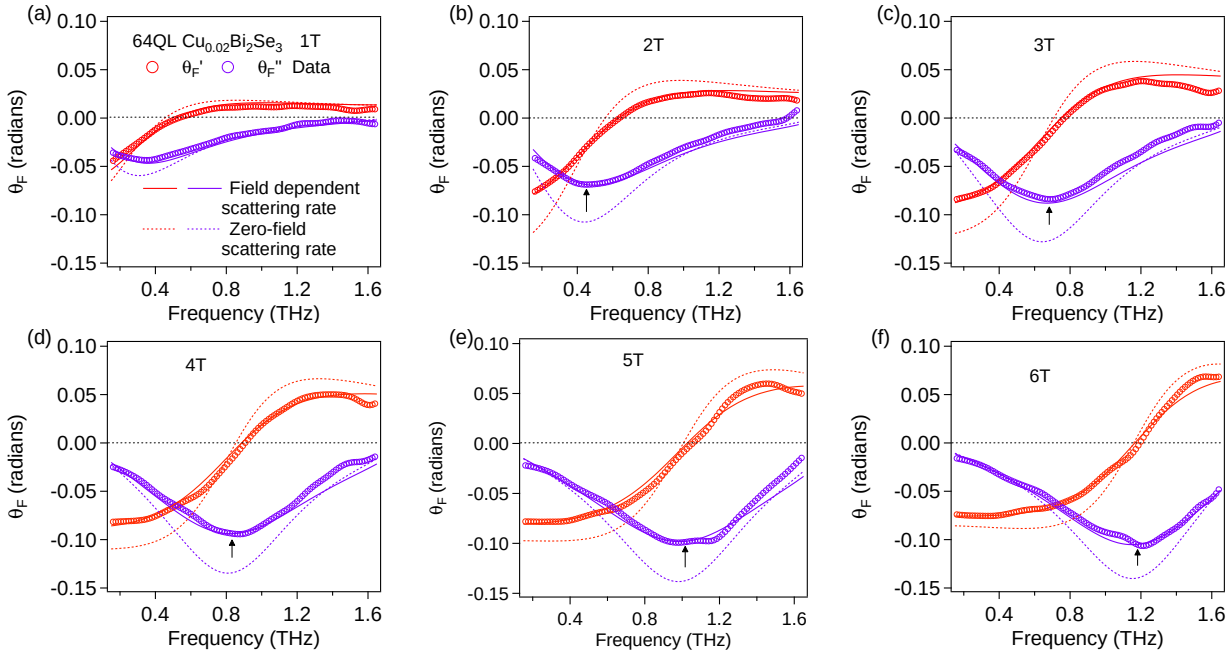


FIG. 2: (Color online) Fit quality on 64QL $Cu_{0.02}Bi_2Se_3$ (sample 1) at different fields. Arrows are eye guides for the cyclotron frequency. Accurate numbers were determined by fits. Solid lines are fits with field-dependent scattering rate. Dashed lines are fits with zero-field scattering rate.

The carrier density of each TSS can be calculated by the usual relation $n_{2D} = k_F^2/4\pi$. An effective transport mass $m^* = \hbar k_F/v_F$ can still be defined for even for 'massless' Dirac fermions where the Fermi velocity is determined by $v_F = \partial E_F/\hbar\partial k$. In our analysis we will consider up to quadratic dispersion for surface states ($E = Ak_F + Bk_F^2$) and model the two surface states as identical with same carrier density. Considering the TSS dispersion up to quadratic correction, the spectral weight can be expressed in terms of $k_F$.

$$\frac{2}{\pi\epsilon_0}\int G_1 d\omega = \omega_p^2 d = \frac{k_F(A + 2Bk_F)e^2}{2\pi\hbar^2\epsilon_0} \tag{2}$$

Therefore, lower spectral weight means lower $k_f$. Lower $k_f$ means lower carrier density and smaller mass. By fitting zero-field conductance, we find $\omega_p^2 d$ in 64QL $Cu_{0.02}Bi_2Se_3$ sample 1 (the one discussed in main text) equal to 3.0±0.2 × $10^4$ $THz^2$ · nm. By using Eq.2, we obtain $k_F \sim 0.06$Å$^{-1}$, $E_F$ = 145 ±5 meV, $m^*$ =0.135±0.05$m_e$ and a total sheet carrier density $n_{2D}$=5.0 ±0.3 ×$10^{12}$/$cm^2$. From Faraday rotation fit, we get the spectral weight $\omega_p^2 d = 2.8 \pm 0.1 \times 10^4$ $THz^2$· nm more accurately. By using the relation $\omega_p^2 d = \frac{n_{2D}e^2}{m^*\epsilon_0}$ and effective mass from CR experiments, we can get carrier density $n_{2D} = 4.9 \pm 0.1 \times 10^{12}/cm^2$. These two analysis agree self-consistently.

Here we show all the data and fits for both 64QL $Cu_{0.02}Bi_2Se_3$ samples (sample 1 and sample 2) . One can see in Fig.2 for $Cu_{0.02}Bi_2Se_3$ (sample 1) that the fit difference between field independent and field dependent scattering rates becomes larger with increasing field, which is another indication of increasing scattering rate with magnetic field.

We observed similar phenomena on another 64QL $Cu_{0.02}Bi_2Se_3$ (sample 2) and reached a similar conclusion to sample 1. This sample 2 remained bulk-insulating and with high mobility after 8 months of exposure to air, which demonstrates realization of a robust bulk-insulating TI by the protection of Se capping. This sample also had $\sim 5.0 \times 10^{12}/\mathrm{cm}^2$ but slightly lower mobility $\sim 2800\ \mathrm{cm}^2/\mathrm{V}\cdot$ s. Data and fitting results are shown in Fig.3. Here we subtracted a small background from the zero-field data, which gives the same result as a substrate background is subtracted. We also performed extended Drude analysis and conclusion is similar to sample 1. We also observed suppression of the scattering rate at low frequency and a coupling constant $\lambda \sim 1.2 \pm 0.3$.

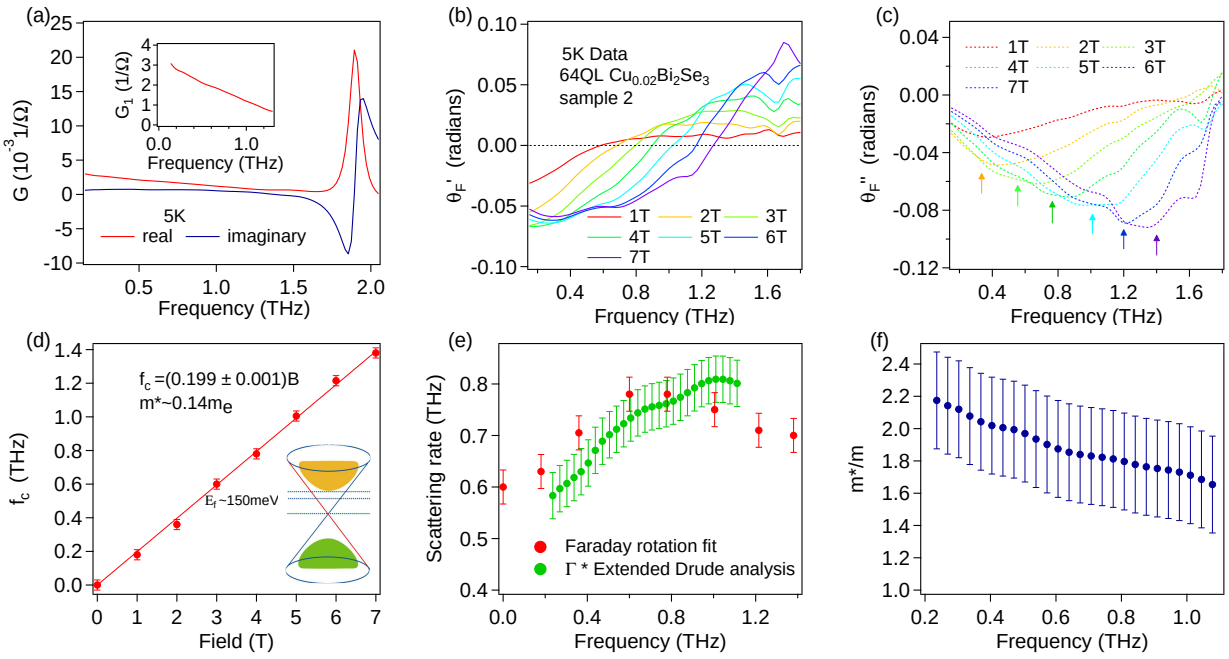


FIG. 3: (Color online) Data summary on 64QL $Cu_{0.02}Bi_2Se_3$ (sample 2) which was exposed in air for 8 months. (a) Complex conductance at 5K. Inset is enlarged real conductance (b) Real and (c) Imaginary part of complex Faraday rotation data at different fields at 5K. (d)Cyclotron frequency versus field. The inset is a cartoon indicating $E_F = 150meV$, 70mev below conduction band minimum. (e) Scattering rate as a function of cyclotron frequency (red). Renomalized scattering rate by mass through extended Drude analysis (green). (f) Renormalized mass as a function of frequency. The error bars express the uncertainty in $\omega_p$ .

In Fig. 4, we show the fits for 100QL $Bi_2Se_3$. This demonstrates that one channel is the principle contribution to the CR and dominates the Faraday rotation. This channel has spectral weight $\omega_p^2 d = 7.6 \pm 0.3 \times 10^4\ \mathrm{THz}^2 \cdot \mathrm{nm}$. We use the spectral weight ( $\omega_p^2 d = \frac{n_{2D}e^2}{m^*\epsilon_0}$) and CR mass 0.20 $m_e$ to extract a total sheet carrier density $n_{2D} \sim 1.9 \pm 0.1 \times 10^{13}/\mathrm{cm}^2$. If using Eq. 2 with the TSS dispersion, from spectral weight we find $k_F \sim 0.11\text{Å}^{-1}$, $E_F \sim 350$ meV, $n_{2D} \sim 2.0 \times 10^{13}/\mathrm{cm}^2$ and $m^* \sim 0.20 m_e$. These two analysis agree again. The second channel gives a low flat background. In the fits of 100QL $Bi_2Se_3$, we fixed the scattering rate of the low mobility channel to 4 THz as we obtained from zero-field conductance fits, but the fits are reasonably insensitive to the precise scattering rate of this channel. Field dependent scattering of the TSS channel of the 100QL $Bi_2Se_3$ is shown in Fig. 5 and the same basic physics as $Cu_{0.02}Bi_2Se_3$ was seen.

A 32QL $Bi_2Se_3$ was also measured. Data summary is shown as Fig.6 The channel that dominates CR has an effective mass $\sim 0.19 m_e$ ,carrier density $\sim 1.90 \times 10^{13}/\mathrm{cm}^2$ and mobility $\sim 2000\ \mathrm{cm}^2/\mathrm{V}\cdot s$, which is consistent with TSSs with $E_f \sim 310$meV above the Dirac point. The chemical potential agrees with ARPES measurements on similar samples[8]. A second channel with scattering rate $\sim 4$ THz is added to fit zero-field conductance. By using the effective mass of bulk/2DEG from literature, the second channel has total sheet carrier density $\sim 0.8 \times 10^{13}/\mathrm{cm}^2$ and mobility less than $300\ \mathrm{cm}^2/\mathrm{V}\cdot s$.

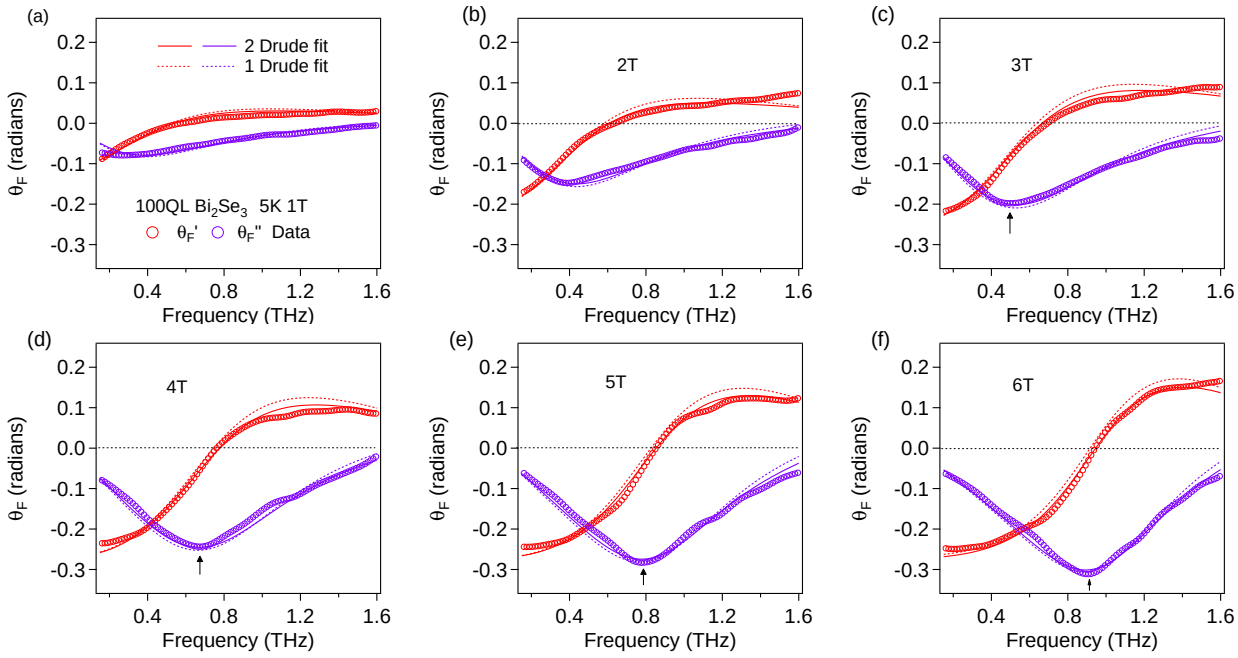


FIG. 4: (Color online) Fit quality on 100QL $Bi_2Se_3$ at different fields. The solid curve is the two Drude fit. Dashed curve is one Drude fit. Arrows are eye guides for the cyclotron frequencies. Accurate numbers are determined by fits.

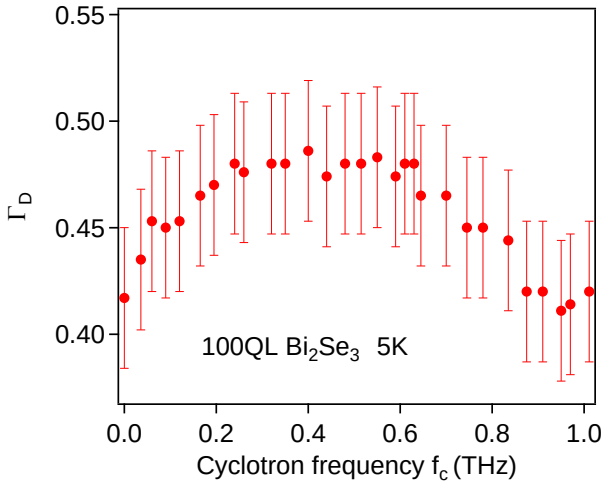


FIG. 5: (Color online) Drude scattering rate of 100QL $Bi_2Se_3$ as a function of cyclotron frequency at 5K.

## III. ZEEMAN (SPIN) EFFECT ON TRANSPORT LIFETIME OF TOPOLOGICAL INSULATORS IN AN EXTERNAL MAGNETIC FIELD

In principle the canting of spins in the surfaces states due to Zeeman coupling under applied field can cause an increase in the scattering rate because backscattering can then occur. In practice this is a very small effect at the current chemical potential levels. One can see this as follows.

The Hamiltonian of the topological insulator surface states is

$$H_k = v\boldsymbol{\sigma} \times \boldsymbol{k}, \tag{3}$$

where $\boldsymbol{k}$ is the electron momentum, $v$ is the Fermi velocity, and $\boldsymbol{\sigma}$ is the Pauli matrix vector corresponding to the spin degrees of freedom.

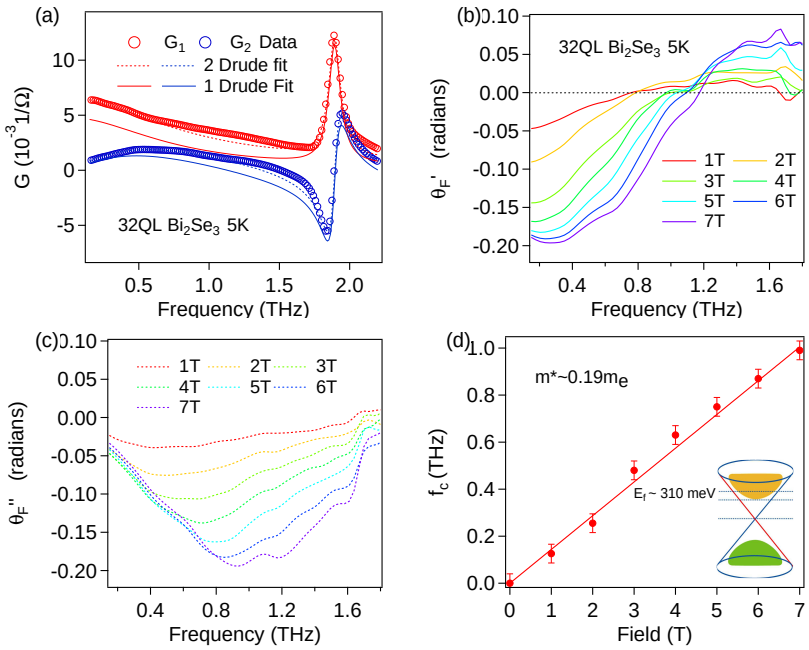


FIG. 6: (Color online) Data summary on 32QL $Bi_2Se_3$ at 5K. (a) Complex conductance at 5K. Solid lines are 1 Drude fits using parameters obtained from fitting the Faradary rotation with 1 Drude term. Dashed lines are 2 Drude fit. (b)Real and (c) Imaginary Faraday rotation at different fields. (d) Cyclotron frequencies as a function of field. Solid line is a linear fit of $f_c = eB/2\pi m^*$. The inset is a cartoon indicating $E_F = 310meV$.

We now introduce an external out-of-plane magnetic field $\boldsymbol{B} = \nabla \times \boldsymbol{A}$, with $\boldsymbol{A}$ the corresponding vector potential. In addition to the orbital coupling given by $\boldsymbol{k} \to \boldsymbol{k} - e\boldsymbol{A}/c$, the Zeeman coupling gives rise to a Dirac mass term $\Delta = -g_s\mu_B B/2$ in the Hamiltonian Eq. (8). In low magnetic fields, we can derive the magnetic field dependence of the transport lifetime $\tau_{tr}$ using the quantum kinetic theory. In this regime, the transport scattering rate $1/\tau_{tr} \ll \omega_c, |\Delta|$ is small compared to the cyclotron frequency $\omega_c = eBv/\hbar k_F$ ($k_F$ is the Fermi wave vector) and the Zeeman splitting $|\Delta|$. The kinetic equation for the momentum-dependent charge-spin density matrix $f_k$ is [9]

$$\frac{\partial f_k}{\partial t} + i[H_k + \Delta\sigma_z, f_k] + \frac{1}{2}\left[e\boldsymbol{E} + \frac{e}{c}\boldsymbol{v}_k \times \boldsymbol{B}, \frac{\partial f_k}{\partial \boldsymbol{k}}\right]_+ = J(f_k|\boldsymbol{k}, t), \tag{4}$$

where $\boldsymbol{E}$ is the external A.C. electric field from the incident light, $\boldsymbol{v}_k = \partial H_k/\partial \boldsymbol{k} = v(\hat{\boldsymbol{z}} \times \boldsymbol{\sigma})$ is the velocity operator, and $[\ ,\ ]_+$ stands for the anti-commutator. $J(f_k|\boldsymbol{k}, t)$ is the collision integral that contains the information about scattering rates. The orbital coupling to the field gives rise to the cyclotron motion which does not flip spins, and therefore does not contribute to the transport lifetime. However, the Zeeman coupling mixes different spins and opens up a spin-flipping channel through electron-impurity scattering. Therefore, at weak magnetic fields, the dependence on $B$ in the collision integral only arises from the Zeeman coupling $\Delta$. A related problem was studied in the literature in the context of the anomalous Hall effect of topological insulators due to magnetic impurities [10, 11]. In the following, we recapitulate the approach in Ref. [10, 11] and obtain the transport lifetime in the presence of Zeeman coupling to the external magnetic field. First we introduce notations $\sin\theta_k = vk/\varepsilon_k$ and $\cos\theta_k = \Delta/\varepsilon_k$ with $\varepsilon_k = \sqrt{(vk)^2 + \Delta^2}$ to rewrite the Zeeman-split Hamiltonian as $H_k = \varepsilon_k \hat{\boldsymbol{e}}_k^{\parallel} \cdot \boldsymbol{\sigma}$, where $\hat{\boldsymbol{e}}_k^{\parallel} = \sin\theta_k(\hat{\boldsymbol{k}} \times \hat{\boldsymbol{z}}) + \cos\theta_k \hat{\boldsymbol{z}}$. We will also need the other two vectors that are orthogonal to $\hat{\boldsymbol{e}}_k$: $\hat{\boldsymbol{e}}_k^{\perp,1} = \hat{\boldsymbol{k}}$ and $\hat{\boldsymbol{e}}_k^{\perp,2} = -\cos\theta_k(\hat{\boldsymbol{k}} \times \hat{\boldsymbol{z}}) + \sin\theta_k \hat{\boldsymbol{z}}$. Then, writing the density matrix $f_k = f_k^{(0)} + \delta f_k$, where $f_k^{(0)}$ is the equilibrium distribution function and $\delta f_k$ is the non-equilibrium part, we can facilitate the solution of Eq. (4) by resolving $\delta f_k$ into components of the projected Pauli matrices $\sigma_{\parallel} = \boldsymbol{\sigma} \cdot \boldsymbol{e}_k^{\parallel}, \sigma_{\perp,1} = \boldsymbol{\sigma} \cdot \hat{\boldsymbol{e}}_k^{\perp,1}, \sigma_{\perp,2} = \boldsymbol{\sigma} \cdot \hat{\boldsymbol{e}}_k^{\perp,2}$: $\delta f_k = n_k + s_k^{\parallel}\sigma_{\parallel} + s_k^{\perp,1}\sigma_{\perp,1} + s_k^{\perp,2}\sigma_{\perp,2}$. The component $n_k$ describes the charge density distribution whereas $s_k^{\parallel}, s_k^{\perp,1}, s_k^{\perp,2}$ respectively describe the distributions of spins projected along the vectors $\hat{\boldsymbol{e}}_k^{\parallel}, \hat{\boldsymbol{e}}_k^{\perp,1}, \hat{\boldsymbol{e}}_k^{\perp,2}$. In particular, $s_k^{\perp,1}, s_k^{\perp,2}$ describe quantum coherence effects that contribute to corrections of higher order in $1/\varepsilon_F\tau_{tr}$ in the conductivity. For the semiclassical weak-field regime we are interested in, the Drude response is given by the conductivity to leading order in $1/\varepsilon_F\tau_{tr}$, and the transport lifetime is therefore determined only by the dynamics of $n_k$ and $s_k^{\parallel}$, but not $\sigma_k^{\perp,1}, \sigma_k^{\perp,2}$. Projecting the collision integral $J(f_k|\boldsymbol{k}, t)$ onto the

charge sector and the "parallel-spin" sector $\sigma_{\parallel}$, the relaxation rate of $n_k$ and $s_k^{\parallel}$ can be calculated as

$$\frac{1}{\tau_k} = \frac{n_i \varepsilon_k}{4v^2} \int_0^{2\pi} \frac{\mathrm{d}\phi_{k'k}}{2\pi} |u(k, \phi_{k'k})|^2 \, (1 - \cos\phi_{k'k}) \left(1 + \cos^2\theta_k + \sin^2\theta_k \cos\phi_{k'k}\right), \tag{5}$$

where $\phi_{k'k}$ is the angle between the momenta $\boldsymbol{k}$ and $\boldsymbol{k}'$, $n_i$ is the impurity concentration and $|u(k, \phi_{k'k})|^2$ is the disorder-averaged impurity potential correlator evaluated at momentum $k' = k$. In the absence of a magnetic field such that $\Delta = 0$, the angular form factor in Eq. (5) reduces to the standard expression $(1 - \cos^2\phi_{k'k})$ which describes suppression of backscattering.

We can model the impurity potential as short-range delta-function scatterers with $|u(k, \phi_{k'k})|^2 \equiv u_0^2$ becoming independent of $k$. The transport lifetime is determined by Eq. (5) at the Fermi level at low temperatures $\varepsilon_F \gg k_B T$. Evaluating the angular integral, we finally obtain the transport lifetime in the weak magnetic field regime

$$\frac{1}{\tau_{tr}} = \frac{n_i u_0^2 \varepsilon_F}{8v^2} \left[1 + 3\left(\frac{g_s \mu_B B}{2\varepsilon_F}\right)^2\right]. \tag{6}$$

Denoting the zero-field transport time as $1/\tau_{tr,0} = n_i u_0^2 \varepsilon_F / 8v^2$, we can see that the weak-field transport lifetime $1/\tau_{tr,B}$ is related to that in zero field as

$$\frac{1}{\tau_{tr,B}} = \frac{1}{\tau_{tr,0}} \left[1 + 3\left(\frac{g_s \mu_B B}{2\varepsilon_F}\right)^2\right]. \tag{7}$$

If we use $g_s \sim 50$, $\epsilon_f \sim 150$meV, the spin effect only gives 0.03 % increases at 1 T. Therefore, we do not think Zeeman effect is the cause for increasing of scattering rate.

## IV. ORBITAL EFFECT ON TRANSPORT LIFETIME OF TOPOLOGICAL INSULATORS IN AN EXTERNAL MAGNETIC FIELD

Here we investigated whether or not the formation of Landau levels can cause a substantial change in the scattering rate.

The Hamiltonian of the topological insulator surface states is

$$H = v\boldsymbol{\sigma} \cdot (\boldsymbol{k} \times \hat{\boldsymbol{z}}), \tag{8}$$

where $\boldsymbol{k}$ is the electron momentum, $v$ is the Fermi velocity, and $\boldsymbol{\sigma}$ is the Pauli matrix vector corresponding to the spin degrees of freedom.

We now introduce an external out-of-plane magnetic field $\boldsymbol{B} = B\hat{\boldsymbol{z}} = \nabla \times \boldsymbol{A}$, with $\boldsymbol{A} = Bx\hat{\boldsymbol{y}}$ the corresponding vector potential in the asymmetric gauge. In addition to the orbital coupling given by $\boldsymbol{k} \to \boldsymbol{k} + e\boldsymbol{A}/c$ (where $e > 0$), the Zeeman coupling gives rise to a Dirac mass term $\Delta = -g_s \mu_B B/2$ in the Hamiltonian Eq. (8). For $Bi_2Se_3$, $g_s = 8.4$ from band structure calculations. The second-quantized Hamiltonian can then be written as

$$H = \omega_c (a\sigma_+ + a^\dagger \sigma_-) + \Delta\sigma_z, \tag{9}$$

where $\omega_c = \sqrt{2}v/\ell_B$ is the Dirac-model cyclotron frequency, $a = (\ell_B/\sqrt{2})[\partial/\partial x + (x + x_0)/\ell_B^2]$ is the harmonic-oscillator lowering operator, and $\sigma_\pm = (\sigma_x \pm i\sigma_y)/2$. As usual, $\ell_B = \sqrt{1/eB}$ is the magnetic length and $x_0 = \ell_B^2 k_y$ is the cyclotron orbit center coordinate. The Landau levels are labeled by integers $n$, which for $n \neq 0$ have eigenenergies and eigenspinors (throughout we use an overbar $\overline{\cdots}$ to denote a spinor quantity)

$$\varepsilon_n = \mathrm{sgn}(n)\sqrt{\omega_c |n| + \Delta^2}, \quad \overline{|n\rangle} = \begin{bmatrix} C_{\uparrow n} \||n| - 1\rangle \\ C_{\downarrow n} \||n|\rangle \end{bmatrix}. \tag{10}$$

where $\||n|\rangle$ (without an overbar and $|n|$ is the absolute value of $n$) denotes the harmonic oscillator eigenstate (Fock state), and

$$\begin{aligned} C_{\uparrow n} &= \mathrm{sgn}(n)\sqrt{\varepsilon_{|n|} + \mathrm{sgn}(n)\Delta}/\sqrt{2\varepsilon_{|n|}}, \\ C_{\downarrow n} &= \sqrt{\varepsilon_{|n|} - \mathrm{sgn}(n)\Delta}/\sqrt{2\varepsilon_{|n|}}. \end{aligned} \tag{11}$$

In the $n = 0$ LL, spins are aligned with the perpendicular field so that

$$\varepsilon_0 = -\Delta, \quad \overline{|0\rangle} = \begin{bmatrix} 0 \\ |0\rangle \end{bmatrix}. \tag{12}$$

The influence of impurity scattering on the density of states and transport properties of the electron system can be captured using the self-consistent Born approximation (SCBA) [12, 13]. This approximation captures certain features of Landau level broadening due to disorder and is usually sufficient to describe magnetotransport properties when localization effect is not important. Proceeding similar to Ref. [12, 13], the self-energy matrix $\Sigma$ contains diagonal elements that couple the same Landau level $n$, $\Sigma_{n,n} \equiv \Sigma_d$, and off-diagonal elements that couple opposite Landau levels $n, -n$, $\Sigma_{n,-n} \equiv \Sigma_o$. For delta-correlated disorder potential $\langle U(\boldsymbol{r})U(\boldsymbol{r}')\rangle = n_i u_0^2 \delta(\boldsymbol{r}-\boldsymbol{r}')$, SCBA implies that

$$\Sigma_+ = \omega_c^2 \rho \sum_{n=0}^{N_c} \frac{\varepsilon - \Sigma_-}{(\varepsilon-\Sigma_+)(\varepsilon-\Sigma_-) - \varepsilon_n^2}, \tag{13}$$

$$\Sigma_- = \omega_c^2 \rho \sum_{n=1}^{N_c} \frac{\varepsilon - \Sigma_+}{(\varepsilon-\Sigma_+)(\varepsilon-\Sigma_-) - \varepsilon_n^2}, \tag{14}$$

where we have defined the dimensionless parameter $\rho = n_i u_0^2/(4\pi v^2)$ that characterizes the disorder strength, and $\Sigma_\pm = \Sigma_d \pm \Sigma_o$. Eqs. (13)-(14) define the self-consistency condition from which the self-energy can be solved.

### A. Moderately High Landau level filling, and Negligible Inter-LL Coupling

This is the simplest case with essentially the physics contributed by each single LL. For Fermi energy filling up to a LL $|N| > 0$, if disorder effect are small so that inter-LL coupling is negligible, the sum over $n$ in Eqs. (13)-(14) is contributed predominantly by the $n = N$ term and other terms $n \neq N$ can be neglected. We can set $\Sigma_+ \approx \Sigma_- \equiv \Sigma$ in Eqs. (13)-(14) and obtain

$$\Sigma = \frac{\omega_c^2 \rho}{2} \frac{1}{(\varepsilon - \varepsilon_N - \Sigma)}, \tag{15}$$

Solving yields the retarded self-energy

$$\Sigma = \begin{cases} (1/2)\left[\varepsilon - \varepsilon_N - i\sqrt{\Gamma^2 - (\varepsilon-\varepsilon_N)^2}\right], & \text{for} \quad |\varepsilon - \varepsilon_N| < \Gamma \\ 0, \quad \text{otherwise} \end{cases} \tag{16}$$

where $\Gamma^2 = 2\omega_c^2\rho = n_i u_0^2/(\pi \ell_B^2)$. The density of states follow from $\nu(\epsilon) = -(1/\pi)\sum_{x_0}\sum_N \mathrm{Im} G_N(\varepsilon)$, where $G_N(\varepsilon) = 1/(\varepsilon - \varepsilon_N - \Sigma)$ is the Green function, and $G_N(\varepsilon) = 4\Sigma/\Gamma^2$ following from Eq. (15). Substituting the self-energy Eq. (16) and suming over the LL degeneracy $\sum_{x_0}\{...\} = 1/(2\pi\ell_B^2)$ gives

$$\nu(\varepsilon) = \frac{1}{\pi^2 \ell_B^2 \Gamma} \sum_N \sqrt{1 - \left(\frac{\varepsilon - \epsilon_N}{\Gamma}\right)^2}\, \theta\left(\Gamma - |\varepsilon - \varepsilon_N|\right), \tag{17}$$

where $\theta(x) = 1$ for $x \geq 0$ and 0 for $x < 0$ is the unit step function. Eq. (17) describes a semi-elliptical shape of the density of states of each LL, which cuts off sharply at $|\varepsilon - \varepsilon_N| = \Gamma$. This is of course only an approximation to the real profile of a disorder broadened LL, which never cuts off sharply and tails off more gradually. The tail parts are what correspond to the localized states in the broadened LL. Therefore, when localization effect to transport is not important, SCBA is a sufficient approximation to high-field transport. In particular, it should capture the dependence of the transport coefficients on $B$ accurately. As shown in the RMP [14], the transport lifetime is proportional to the density of states. Eq. (17) predicts an overall trend for $\nu(\epsilon)$ that increases with $B$, therefore the transport lifetime should also increase with $B$ in this moderately high LL filling with negligible inter-LL coupling effect from disorder. Since the experimental data does not show an increasing trend at the higher end of the magnetic field range, in our opinions this is probably not the regime where the sample was at $4 - 7$ T. We have furthermore checked the case of an "improvised" SCBA where people replace the semi-elliptical density of states with a Gaussian one to better capture the effects of localization (which were found to be in better agreement with magneto-transport experiments in GaAs quantum wells), the overall dependence of $B$ is still increasing, so it does not change our conclusion in this section.

### B. High LL with Inter-LL Coupling—Magneto-oscillations in transport lifetime

For LL disorder broadening $1/\tau_q$ large such that $\omega_c \tau_q \ll 1$ (but $1/\tau_q > 1/\tau_{tr}$ so $1/\tau_{tr}$ could be $\lesssim \omega_c$), this regime corresponds to sdH magneto-oscillations. For a LL filling $|N| > 0$, we have $\Sigma_+ \approx \Sigma_- \equiv \Sigma$ in Eqs. (13)-(14)

$$\Sigma = \omega_c^2 \rho \sum_{n=0}^{N_c} \frac{\varepsilon - \Sigma}{(\varepsilon-\Sigma)^2 - \varepsilon_n^2}, \tag{18}$$

Furthermore, for high LL filling $|N| \gg 1$, one can use the approximation of extending the lower limit of the sum to $-N_c$ and setting $N_c \to \infty$, because the main contribution comes from the Fermi level and contributions from negative LLs and from $N$ to $\infty$ amount to negligible errors. This is a standard trick in going to the weaker-field regime from the strong-field LL sum formula to obtain the magneto-oscillatory behavior.

Consider the sum in Eq. (18), using the Poisson summation formula, we obtain

$$\sum_{n=-\infty}^{n=\infty} F(n) = \frac{\pi}{\omega_c^2}(\varepsilon - \Sigma)\cot\left\{\frac{\pi}{\omega_c^2}\left[(\varepsilon-\Sigma)^2 - \Delta^2\right]\right\}, \tag{19}$$

Expanding $\cot(\pi z)$ into a Fourier series,

$$\cot(\pi z) = -i\left[1 + 2\sum_{k=1}^{\infty} e^{i2\pi k z}\right], \tag{20}$$

(valid for $\mathrm{Im} z > 0$) and writing the retarded self-energy as $\Sigma = \Sigma' + i\Sigma''$ where $\Sigma'$ and $\Sigma'' < 0$ are the real and imaginary parts of the retarded self-energy, Eq. (18) becomes

$$\begin{aligned}\Sigma' + i\Sigma'' &= -i\pi\rho\,(\varepsilon - \Sigma' - i\Sigma'') \\ &\times\left\{1 + 2\sum_{k=1}^{\infty}\exp\left\{i\frac{2\pi k}{\omega_c^2}\left[\varepsilon^2 - \Delta^2 - 2\varepsilon\Sigma' + (\Sigma')^2 - (\Sigma'')^2 - i2\Sigma''(\varepsilon - \Sigma')\right]\right\}\right\},\end{aligned} \tag{21}$$

Eq. (22) is a nonlinear equation that needs to be solved iteratively. The small parameter here is the so-called Dingle factor which is the real part of the expression inside the sum

$$\lambda = \exp\left\{-\frac{4\pi}{\omega_c^2}|\Sigma''|\,(\varepsilon - \Sigma')\right\}. \tag{22}$$

So we can write Eq. (22) as

$$\Sigma' + i\Sigma'' = -i\pi\rho\,(\varepsilon - \Sigma' - i\Sigma'')\left\{1 + 2\sum_{k=1}^{\infty}\lambda^k \exp\left\{i\frac{2\pi k}{\omega_c^2}\left[(\varepsilon-\Sigma')^2 - \Delta^2 - (\Sigma'')^2\right]\right\}\right\}, \tag{23}$$

and solve for $\Sigma$ up to first order in disorder correlation $\sim n_i u_0^2$ ($O(\rho^1)$) and to first order in $\lambda$ ($O(\lambda^1)$).

In the zeroth order $O(\lambda^0)$, we have $\Sigma' = 0$ and $\Sigma'' = -(n_i u_0^2/4v^2)\varepsilon$, the latter can be identified as the quasiparticle scattering rate $1/2\tau_{q,0} = (n_i u_0^2/4v^2)\varepsilon$ at zero magnetic field.

To first order $O(\lambda^1)$, we obtain

$$\begin{aligned}\Sigma' &= \frac{1}{\tau_{q,0}}\varepsilon\lambda\sin\left[2\pi\left(\frac{\varepsilon^2-\Delta^2}{\omega_c^2}\right)\right], \\ \Sigma'' &= -\frac{1}{2\tau_{q,0}}\left\{1 + 2\lambda\cos\left[2\pi\left(\frac{\varepsilon^2-\Delta^2}{\omega_c^2}\right)\right]\right\}.\end{aligned} \tag{24}$$

The density of states is $\nu(\varepsilon) = -(1/2\pi^2\ell_B^2)\mathrm{Im}\sum_{n=-N_c}^{N_c}\mathrm{Im}G_n(\varepsilon)$. For the present high LL regime, the contribution from the zeroth LL is small, and $\nu(\varepsilon) \simeq 2\sum_{n=0}^{N_c}(\varepsilon-\Sigma)/[(\varepsilon-\Sigma)^2 - \varepsilon_n^2]$, which is equal to $2\mathrm{Im}\Sigma/\omega^2\rho$ according to the SCBA equation Eq. (18). Therefore

$$\nu(\varepsilon) = \nu_0(\varepsilon)\left\{1 + 2\lambda\cos\left[2\pi\left(\frac{\varepsilon^2-\Delta^2}{\omega_c^2}\right)\right]\right\}, \tag{25}$$

with $\nu_0(\varepsilon) = \varepsilon/2\pi v^2$ being the density of states at zero magnetic field.

The ratio of the transport scattering rate at finite field to that at zero field is equal to that of the density of states [14], and finally we have

$$\frac{1}{\tau_{tr,B}} = \frac{1}{\tau_{tr,0}}\left\{1 + 2\lambda\cos\left[2\pi\left(\frac{\varepsilon_F^2 - (g_s\mu_B B/2)^2}{\omega_c^2}\right)\right]\right\}, \tag{26}$$

where $1/\tau_{tr,0} = n_i u_0^2\varepsilon_F/4v^2$ is the transport time at zero field.

If we are in this scenario, scattering rate should show oscillation above 3T when $\omega\tau = f_c\Gamma \geq 1$. We also rule out this possibility.

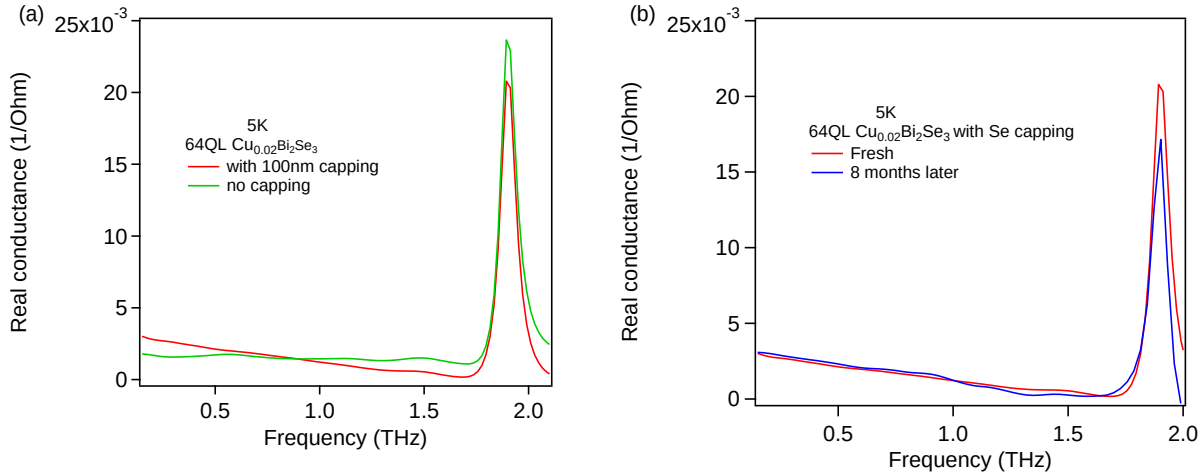


FIG. 7: (Color online) (a) Real conductance of 64QL $Cu_{0.02}Bi_2Se_3$ (sample 2) with and without 100nm Se capping at 5K . (b) Real conductance of 64QL $Cu_{0.02}Bi_2Se_3$ (sample 2) with 100nm Se capping right measured right after growth and 8 month later.

## V. EFFECT OF SE CAPPING

Our previous work on pure $Bi_2Se_3$ showed that Se capping had a negligible effect on the optical properties of $Bi_2Se_3$, but does decrease the scattering rate somewhat. However, it is of great importance in the present case of Cu doped $Bi_2Se_3$ as these samples are very air sensitive. Transport measurements in Ref.[5] were performed within 20 mins after samples were taken out of ultra-high vacuum MBE chamber. Samples for THz measurements were sealed in vacuum bags and shipped overnight to JHU. The total exposure to atmosphere is around 10 mins before loading into the cryostat . As one can see in Fig.7(a), Se capping protects the mobility of the sample well as opposed to non-capped samples with a flat Drude peak. 100nm Se capping still protects the sample well even after 8 months as shown in Fig.7(b).

## VI. VALIDITY OF ONE DRUDE COMPONENT FIT IN PREVIOUS WORK[1, 2]

For the 100QL $Bi_2Se_3$ sample, fitting zero field conductance data by a single Drude term, a phonon term and a $\epsilon_\infty$ term, we find the Drude spectral weight is $\omega_p^2 d$ is $4.6\times10^6\ 4\pi^2\text{THz}^2\cdot$ nm. Using Eq. 2, we find $k_F$ ~0.14Å$^{-1}$, $m^*$ ~0.22$m_e$ and $E_F$ ~480 meV. A fit to the Faraday rotation data alone shows that the spectral weight $\omega_p^2 d$ contributing to the TSSs is $2.8\times10^6\ 4\pi^2\text{THz}^2$nm. Still using Eq. 2, a $k_F$ ~0.11Å$^{-1}$, $m^*$ ~0.20$m_e$ and $E_F$ ~350 meV are obtained, as mentioned above already. One can see $E_F$ and $k_F$ are overestimated by ~ 30%, while $m^*$ is overestimated by ~ 10% if one associates all the Drude spectral weight in the zero-field conductance to the TSSs. These quantities are overestimated in the single Drude component model because one assigns all the bulk/2DEG spectral weight as the TSSs spectral weight. The second Drude channel (bulk/2DEG) is flat in our measurement frequency regime and only contributes a smooth background. However, considering the fact that the TSSs contribute more than 90% to the total conductance, a single Drude model analysis is still a good approximation and a thickness independent Drude peak as observed previously in $Bi_2Se_3$[1, 2] is not surprising. The presence of this very flat subdominant contribution does not call into question any of the conclusions of our previous works [1, 2]. Here we just clarify this point and provide a method to separate contributions from TSSs and bulk/2DEG in magneto-THz measurements.

## VII. EFFECTIVE MASS CONSISTENCY WITH PREVIOUS WORK

In our earlier work[1], a heavier $0.35m_e$ cyclotron mass for TSSs was reported. This was judged to be a reasonable number based on a linear dispersion of the TSSs and using $m^* = E_F/v_F^2$, where $E_F$ ~0.5eV and $v_F = 5\times10^5 m/s$. However, if one considers quadratic corrections the to TSS dispersion, one finds that this mass does not give the right $k_F$. In addition, if we use a linear dispersion $E_F = \hbar v_F k_F$ and use spectral weight to estimate the chemical potential, the relation is $\omega_p^2 d = \hbar v_F k_F e^2/2\pi\epsilon_0\hbar^2 = E_f e^2/2\pi\epsilon_0\hbar^2$ and $E_F$ is ~0.75eV. Therefore, when $E_F$ is in the conduction band, quadratic corrections are significant. The fact that in order that the wave functions of the TSSs vanish at the TI/vacuum interface, a quadratic correction is needed [15, 16]. We believe that the mass given in previous work was incorrect for pure $Bi_2Se_3$ films and the revised value of $0.20m_e$ given in this

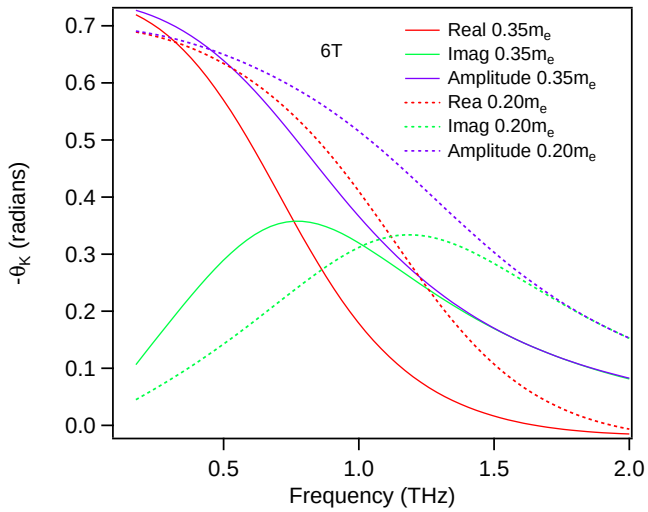


FIG. 8: (Color online) Calculation of Kerr rotation with effective mass $0.35m_e$ and mass $0.20m_e$ with carrier density $n_{2D} = 2 \times 10^{13}/\text{cm}^2$ and scattering rate $\Gamma_D$=1THz at 6T.

work is correct.

The reasons for this correction is multifold. 1.) Signal to noise has been significantly increased in the current generation of experiments [7] allowing more reliable fits to the spectra. 2.) The current generation of $Bi_2Se_3$ films have mobilities of the order 2000 - 3200 $\text{cm}^2/\text{V}\cdot$ s [4]. In order to see a well-defined cyclotron resonance in the dissipative response, the relation $\omega_c\tau = \mu B \geqslant 1$ needs to be satisfied[17]. $\omega_c\tau = \mu B \sim$ 1.5-2 is still too small to see very sharp peaks in the amplitude of Kerr/Faraday rotation in our field range. 3.) In the previous work, due to (now overcome) uncertainties in the measured phase in the fast rotator experiment, only the amplitude of the Faraday rotation was considered reliable. Unfortunately this is a somewhat insensitive method of probing the cyclotron frequency. As one can see from Fig.8, the rotation spectrum does not differ much using $0.35m_e$ or $0.20m_e$ in the amplitude plot. To fit the data accurately when $\omega_c\tau \sim 1$, one needs to fit the complex Faraday rotation; the peak in the imaginary angle approximately gives the cyclotron frequency. In this regard, phase sensitive time-domain THz spectroscopy is a powerful tool to study cyclotron resonances in topological insulators of the current generation. Despite the differences in these numbers, the $Bi_2Se_3$ samples we measured in this paper are similar to those in Ref[1] and the qualitative conclusion that TSSs dominates made in Ref[1] remains.

## VIII. ASSUMPTION OF NEARLY EQUAL CONTRIBUTION OF THE TOP AND BOTTOM SURFACE STATES

In the main text, we showed that the carrier density estimated by using the spectral weight and mass from the Faraday rotation fits is close to the value obtained using spectral weight from Faraday rotation fit and surface state dispersion. This shows the assumption of nearly equal contribution from two surface states is a good approximation. Similarly, ARPES and DC transport showed the chemical potential of the two surface states differed by around 50 meV[18, 19]. Considering the potential fluctuation near the Dirac point [20] is also around 50 meV estimated by previous work[21], the equal contribution is not surprising.

A method was discussed in Ref.[21] to distinguish the contribution of the two surfaces from each other. Unfortunately, it appears that the interface between $In_2Se_3$ and $Bi_2Se_3$ is not as simple as assumed in Ref.[21]. It has been found that there is 20-30% Indium diffusion into the $Bi_2Se_3$ layer in a recent study[22]. The topological phase transition occurs near x$\sim$ 6 % in $(Bi_{1-x}In_x)_2Se_3$[2, 23]. Therefore, the interface of $In_2Se_3$ and $Bi_2Se_3$ is not the boundary of normal band insulator and topological insulator. The true interface TSS must be buried deeply and exist in a background of high disorder. Due to gradient Indium diffusion, the interface which hosts SSs could be $(Bi_{0.045}In_{0.955})_2Se_3$ / $Bi_2Se_3$. This hypothesis can explain that the conduction band minimum is positioned only $\sim$ 80 meV above the Dirac point, because the bulk gap decreases when approaching the topological phase transition point at $x \sim 6$ %. Also, more Indium substitution reduces the total carrier density, which could be the reason that the top surface has a lower carrier density as discussed in Ref.[24]. We also measured a 32QL $Bi_2Se_3$ capped by 10nm $In_2Se_3$. This sample has lower spectral weight and a larger scattering rate, as shown in Fig.9. However, assuming the gate does not affect the back surface, Ref.[24] estimated $\sim 10^{13}/\text{cm}^2$ carrier sits on the back surface. This can be additional support for the assumption of nearly equal contribution of two surface states in normal $Bi_2Se_3$ samples.

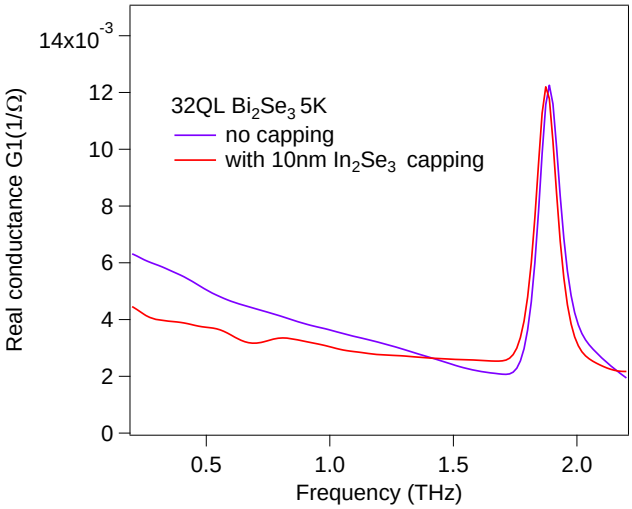


FIG. 9: (Color online) Real conductance of 32QL $Bi_2Se_3$ with and without 10nm $In_2Se_3$ capping at 5K.

## IX. ROLE OF COPPER

The majority of Cu was found to be $Cu^{0+}$ (neutral) by X-ray photo-emission spectroscopy in this batch of samples[5]. Our data also supports this scenario. If 2% Cu substitutes for Bi, then we would observe the shift of phonon frequency as we did in the $(Bi_{1-x}In_x)_2Se_3$ case. In $(Bi_{1-x}In_x)_2Se_3$, we can observe a shift of the phonon at x$\sim$ 1%. Also note that Cu has around half of the atomic number of In, which means 2% Cu substitution would shift the phonon frequency even higher. Normal $Bi_2Se_3$ is known to have a conducting bulk with $E_F \sim$ 350 meV-450 meV due to Se vacancies. Along with Ref.[5],we believe Cu incorporation deactivate Se vacancies so the density is reduced. We encourage more work to be done to resolve the role of copper by other methods such as STM measurements and first-principle calculations.

## X. BAND BENDING

Topological Insulators can be understood as special narrow-gap semiconductors with surface states. Therefore, band bending effects can be important for topological insulators. Ref. [5] has a nice summary about band bending in TIs. Here we re-emphasize its importance. The bulk chemical potential for normal $Bi_2Se_3$ is pinned near the conduction band minimum (therefore $\sim$ 230 meV above Dirac point)[5, 25], while the surface state chemical potential is $\sim$ 350 meV in our samples. Downward band bending results in accumulation layers. From magneto-terahertz measurements, we conclude that any accumulation layer carriers have a large scattering rate, are essentially featureless in the Faraday rotation and count for less than 10 % of total conductance. For $Cu_{0.02}Bi_2Se_3$, the chemical potential at the surface is $\sim$ 150 meV the Dirac point, and therefore upwards band bending must occur. ARPES can play an essential role in determining whether a material is a topological insulator by counting if the number of surface state branches is odd or even, but it is not the best tool to conclude whether a TI is bulk-insulating or not due to its extreme surface sensitivity and band bending. For example, upwards band bending was reported in bulk-conducting TI[25] where ARPES did not observe bulk states but SdH saw a dominating bulk contribution. The most effective way to probe for bulk-insulating TIs is through transport measurements. In DC transport, if the carrier density contributing to SdH oscillations is equal to the total carrier density measured by the Hall effect, then the bulk is insulating[5]. In AC optics, if the carrier density contributing to cyclotron resonance is equal to the total carrier density in the Drude term of the zero field conductance, one can conclude that the bulk is insulating.

* Electronic address: npa@pha.jhu.edu

[1] R. Valdés Aguilar, A. V. Stier, W. Liu, L. S. Bilbro, D. K. George, N. Bansal, L. Wu, J. Cerne, A. G. Markelz, S. Oh, et al., Phys. Rev. Lett. **108**, 087403 (2012).

[2] L. Wu, M. Brahlek, R. V. Aguilar, A. V. Stier, C. M. Morris, Y. Lubashevsky, L. S. Bilbro, N. Bansal, S. Oh, and N. P. Armitage, Nature Physics **9**, 410 (2013).
[3] N. Bansal, Y. Kim, M. Brahlek, E. Edrey, and S. Oh (2011), arxiv:1104.5709.
[4] N. Bansal, Y. Kim, M. Brahleck, E. Edrey, and S. Oh, Phys. Rev. Lett. **109**, 116804 (2012).
[5] M. Brahlek, N. Koirala, M. Salehi, N. Bansal, and S. Oh, Phys. Rev. Lett. **113**, 026801 (2014).
[6] R. Valdés Aguilar, L. Wu, A. V. Stier, L. S. Bilbro, M. Brahlek, N. Bansal, S. Oh, and N. P. Armitage, J. Appl. Phys. **113**, 153702 (2013).
[7] C. Morris, R. Valdés Aguilar, A. Stier, and N. Armitage, Optics Express **20**, 12303 (2012).
[8] Y. Cao, J. Waugh, X. Zhang, J. Luo, Q. Wang, T. Reber, S. Mo, Z. Xu, A. Yang, J. Schneeloch, et al., Nature Physics **9**, 499 (2013).
[9] O. E. Raichev and F. T. Vasko, *Quantum Kinetic Theory and Applications* (Springer, 2005).
[10] D. Culcer and S. Das Sarma, Phys. Rev. B **83**, 245441 (2011).
[11] D. Culcer, E. H. Hwang, T. D. Stanescu, and S. Das Sarma, Phys. Rev. B **82**, 155457 (2010).
[12] N. H. Shon and T. Ando, Journal of the Physical Society of Japan **67**, 2421 (1998).
[13] Y. Zheng and T. Ando, Phys. Rev. B **65**, 245420 (2002).
[14] I. Dmitriev, A. Mirlin, D. Polyakov, and M. Zudov, Reviews of Modern Physics **84**, 1709 (2012).
[15] C.-X. Liu, X.-L. Qi, H. Zhang, X. Dai, Z. Fang, and S.-C. Zhang, Phys. Rev. B **82**, 045122 (2010).
[16] G. Refael (2014), privite Communication.
[17] J. Kono and N. Miura, High Magnetic Fields: Science and Technology, Volume III, World Scientific, Singapore (2006).
[18] Y. Zhang, K. He, C. Chang, C. Song, L. Wang, X. Chen, J. Jia, Z. Fang, X. Dai, W. Shan, et al., Nature Physics **6**, 584 (2010).
[19] Y. Xu, I. Miotkowski, C. Liu, J. Tian, H. Nam, N. Alidoust, J. Hu, C.-K. Shih, M. Z. Hasan, and Y. P. Chen, Nature Physics **10**, 956 (2014).
[20] H. Beidenkopf, P. Roushan, J. Seo, L. Gorman, I. Drozdov, Y. Hor, R. J. Cava, and A. Yazdani, Nat. Phys. **7**, 939 (2011).
[21] G. S. Jenkins, D. C. Schmadel, A. B. Sushkov, H. D. Drew, M. Bichler, G. Koblmueller, M. Brahlek, N. Bansal, and S. Oh, Phys. Rev. B **87**, 155126 (2013).
[22] H. Lee, C. Xu, S. Shubeita, M. Brahlek, N. Koirala, S. Oh, and T. Gustafsson, Thin Solid Films **556**, 322 (2014).
[23] M. Brahlek, N. Bansal, N. Koirala, S.-Y. Xu, M. Neupane, C. Liu, M. Z. Hasan, and S. Oh, Phys. Rev. Lett. **109**, 186403 (2012).
[24] G. S. Jenkins, D. C. Schmadel, A. B. Sushkov, H. D. Drew, M. Bichler, G. Koblmueller, M. Brahlek, N. Bansal, and S. Oh, Phys. Rev. B **87**, 155126 (2013).
[25] J. G. Analytis, J.-H. Chu, Y. Chen, F. Corredor, R. D. McDonald, Z. X. Shen, and I. R. Fisher, Phys. Rev. B **81**, 205407 (2010).